Journal of Nuclear Materials 492 (2017) 269–278

Contents lists available at ScienceDirect

Journal of Nuclear Materials

journal homepage: www.elsevier.com/locate/jnucmat

DFT+U study of the structures and properties of the actinide dioxides

James T. Pegg [a, b, *], Xavier Aparicio-Anglès [a], Mark Storr [b], Nora H. de Leeuw [a, c]

[a] University College London, Department of Chemistry, 20 Gordon Street, London WC1H 0AJ, United Kingdom
[b] Atomic Weapons Establishment (AWE) Plc, Aldermaston, Reading RG7 4PR, United Kingdom
[c] Cardiff University, School of Chemistry, Main Building, Park Place, Cardiff CF1D 3AT, United Kingdom

ARTICLE INFO

Article history:
Received 6 March 2017
Received in revised form
18 May 2017
Accepted 19 May 2017
Available online 23 May 2017

Keywords:
DFT+U
Non-collinear magnetism
Transverse
Longitudinal
Actinide dioxide
Nuclear fuel

ABSTRACT

The actinide oxides play a vital role in the nuclear fuel cycle. For systems where current experimental measurements are difficult, computational techniques provide a means of predicting their behaviour. However, to date no systematic methodology exists in the literature to calculate the properties of the series, due to the lack of experimental data and the computational complexity of the systems. Here, we present a systematic study where, within the DFT+U formulism, we have parametrized the most suitable Coulombic (U) and exchange (J) parameters for different functionals (LDA, PBE, PBE-Sol and AM05) to reproduce the experimental band-gap and lattice parameters for ThO_2, UO_2, NpO_2, PuO_2, AmO_2 and CmO_2. After successfully identifying the most suitable parameters for these actinide dioxides, we have used our model to describe the electronic structures of the different systems and determine the band structures, optical band-gaps and the Bulk moduli. In general, PBE-Sol provides the most accurate reproduction of the experimental properties, where available.

We have employed diamagnetic order for ThO_2, PuO_2 and CmO_2, transverse 3k antiferromagnetic order for UO_2 and AmO_2, and longitudinal 3k antiferromagnetic order for NpO_2. The Fm $\bar{3}$ m cubic symmetry is preserved for diamagnetic ThO_2, PuO_2 and CmO_2 and longitudinal 3k NpO_2. For UO_2 and AmO_2, the transverse 3k antiferromagnetic state results in Pa$\bar{3}$ symmetry, in agreement with recent experimental findings. Although the electronic structure of ThO_2 cannot be reproduced by DFT or DFT+U, for UO_2, PuO_2, NpO_2, AmO_2 and CmO_2, the experimental properties are very well represented when U = 3.35 eV, 6.35 eV, 5.00 eV, 7.00 eV and 6.00 eV, respectively, with J = 0.00 eV, 0.00 eV, 0.75 eV, 0.50 eV and 0.00 eV, respectively.

1. Introduction

The study of the actinides is primarily due to their importance in the nuclear fuel cycle [1–3], where actinides are commonly encountered in their oxide form (AnO_2) [4–6]. Compared to the metal, the oxides demonstrate better thermal and chemical stability [7], which is of paramount importance when we are considering nuclear energy applications [5]. The oxides enable higher operating temperatures and guard against further oxidation of the nuclear fuels, thus limiting the risk of containment failure and thermal excursion, and ensuring the stability of spent nuclear material for long-term storage [3,4,8]. It is, however, known, that under specific conditions, the AnO_2 may form hyperoxides of the form AnO_{2+x} [9].

In nuclear fission, fissile isotopes of uranium (^{235}U) and plutonium (^{239}Pu) are used as nuclear fuel [3,10]. Over time the composition of nuclear oxide fuels change, either because of the genesis of irradiation-induced defects [11], or because of the formation of fission products [12]. Actinide oxides of interest include thorium dioxide (ThO_2), neptunium dioxide (NpO_2), americium dioxide (AmO_2), and curium dioxide (CmO_2). Evaluating the properties of these materials has important implications for the development of new processing strategies and the storage of nuclear material, thus improving the generation and safety of nuclear energy [10,12–16].

The study of AnO_2 properties faces several challenges. The actinides are inherently unstable, highly toxic, and, due to the risk of nuclear proliferation, subject to strict regulatory controls [17]. In addition, their experimental investigation is further limited by their low abundance, isolation, and high radioactivity, which has led to

* Corresponding author. University College London, Department of Chemistry, 20 Gordon Street, London WC1H 0AJ, United Kingdom.
E-mail address: uccajtp@ucl.ac.uk (J.T. Pegg).

http://dx.doi.org/10.1016/j.jnucmat.2017.05.025

the lack of precise information on fundamental properties [10,18]. Important properties that require assessment include the lattice constants, band gaps, magnetic states, and the bulk moduli. Theoretical chemistry represents a powerful tool to unequivocally determine these properties, although conventional computational methods, based on density functional theory (DFT), often fail due to the relativistic influences and the highly correlated nature of these materials [19]. Hence, treatment by specific methods that are able to asses this type of material is required.

The following methods have been developed to calculate highly correlated materials: the self-interaction correction method (SIC) [20], modified density functional theory (DFT+U) [20,21], dynamic mean field theory (DMFT) [22], and screened hybrid density functional theory (HSE) [23,24]. Among these methodologies, DFT+U represents one of the more computationally tractable means of study, since it offers the possibility to accurately reproduce the properties of highly correlated materials at a reasonable computational cost [1]. This is achieved by manipulating the so-called Hubbard Coulombic (U) and exchange (J) modifiers, thus minimizing the DFT self-interaction error (SIE). However, U and J have to be fitted to experimental data, and for actinide materials, relativistic effects must also be taken into account. This is the reason why, to the best of our knowledge, few theoretical reports have been published so far that consider SOI and noncollinear magnetic order [25–27]. Hence, determining an accurate value of U and J would represent a significant advance, allowing in the exploration of these materials.

In this paper, we perform a systematic study to determine a set of Hubbard parameters for the DFT+U approximation for different functionals and different materials. Past studies have so far limited themselves to discussion of LDA, PW91, PBE or hybrid functionals. To the authors' knowledge, this is the first study of the AnO_2 systems that investigates the performance of the more current AM05 and PBE-Sol functionals. In previous work in the literature, these functionals have been shown to improve calculations of transition metal complexes in terms of the lattice constant and surface energetics [28,29]. It is thus important that their application to AnO_2 systems is evaluated as well. In addition, we have chosen to implement the magnetic state determined from experimental procedure and/or predicted from the one electron crystal field (CF) and Russel-Saunders coupling scheme [25]. Our paper aims to address the issues encountered in the computational modelling of actinide-based materials to provide a basis on which further research can be built.

1.1. Magnetic structure

In Fig. 1, under standard conditions, the AnO_2 crystallise in the calcium fluorite (CaF_2) structure with $Fm\bar{3}$ m (No. 225) symmetry [14,30–33]. The lattice resembles that of an actinide face-centred cubic (FCC) structure where oxygen occupies tetrahedral holes. Thus, each actinide (An^{4+}) cation is coordinated to eight oxygen anions (O^{2-}) and each O^{2-} is coordinated to four An^{4+}.

The electronic structure of these materials can be understood from the crystal field (CF) theory. The spin-orbit interaction (SOI) forces the splitting of the single electron *f*-orbitals into two different levels, with j = 7/2 and j = 5/2 respectively. Since each actinide cation has a cubic environment, the degeneracy of these levels is subsequently broken due to the crystal field. Although this approximation is technically valid only for the single *f*-electron case, it is widely used to predict the orbital occupancy [25]. Hence, Th^{4+}, Pu^{4+}, and Cm^{4+} are predicted to have no effective magnetic moment ($\mu_B = 0$), whereas U^{4+}, Np^{4+}, and Am^{4+} present an effective magnetic moment ($\mu_B \neq 0$), as illustrated in Fig. 2.

The display of these magnetic moments in the actinide dioxides

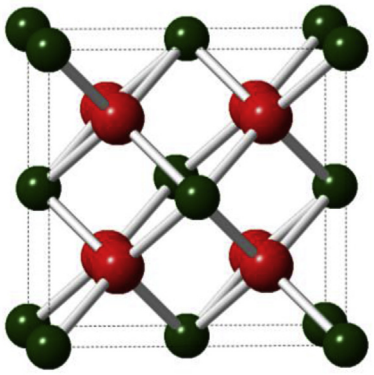

Fig. 1. Representation of the unit cell of an actinide dioxide (AnO_2). An^{4+} ions are coloured in green and O^{2-} ions are coloured in red. (For interpretation of the references to colour in this figure legend, the reader is referred to the web version of this article.)

leads to different magnetic structures. If the ions show no magnetic moment, the resulting structure is the non-ordered diamagnetic (DM) state. In contrast, if the ions do present an effective magnetic moment, we can have two different situations, depending on whether these magnetic moments are coupled or not. If they are decoupled, there is no ordered distribution and this results in the disordered paramagnetic (PM) phase; if ordered or coupled, either ferromagnetic (FM) or antiferromagnetic (AFM) states are obtained. In addition, if magnetic moments are coupled but they show different μ_B, the resulting magnetic structure is known as the ferrimagnetic (FI) state.

Further, the ordered magnetic AnO_2 exhibit non-collinear behaviour [34–37], where the magnetic moments of the ions have contributions in more than one direction. Hence, we distinguish 1k (one wave-vector), 2k (two independent wave-vectors), and 3k (three independent wave-vectors) magnetic wave vectors [37,38]. Specifically, AnO_2 are non-collinear 3k AFM materials. For the AFM 3k phase, one can distinguish between three different phases: the longitudinal 3k AFM, and the two equivalent transverse 3k AFM domains (A and B), depicted in Fig. 3.

The non-ordered magnetic systems are relatively simple to calculate compared to their ordered non-collinear magnetic counterparts. Experimentally, for ThO_2 [39] and PuO_2 [40–44] diamagnetism has been confirmed. It is worth noting, however, that there is a controversy over the exact magnetic ground state for PuO_2, where first-principles methods have suggested the possibility of an AFM ground state [25]. However, for this work we have assumed the DM ground state, as supported by the complete active space self-consistent field (CASSCF) [45] method and experimental evidence [40,42–44]. CmO_2 has been reported as PM, although according to CF theory, it should be DM. It is believed that the presence of impurities plus the small energy difference between the DM and the PM phases in CmO_2 are the reason the DM phase has been difficult to determine [12,46]; here, we have again assumed a DM ground state for CmO_2.

The ordered magnetic AnO_2 have attracted considerable interest, in part due to their non-trivial multi-k and multipolar nature. In UO_2, the magnetic ground state is identified as a transverse 3k AFM [47] state at $T_N = 30.8$ K [48] (where T_N is the Neel Temperature for an AFM-PM magnetic transition) with a corresponding effective magnetic moment of 1.74 μ_B/U ion. In addition, neutron studies have indicated an internal oxygen displacement; although no external distortion of the cubic structure occurs [49]. One theoretical study has employed SOI to investigated the relative

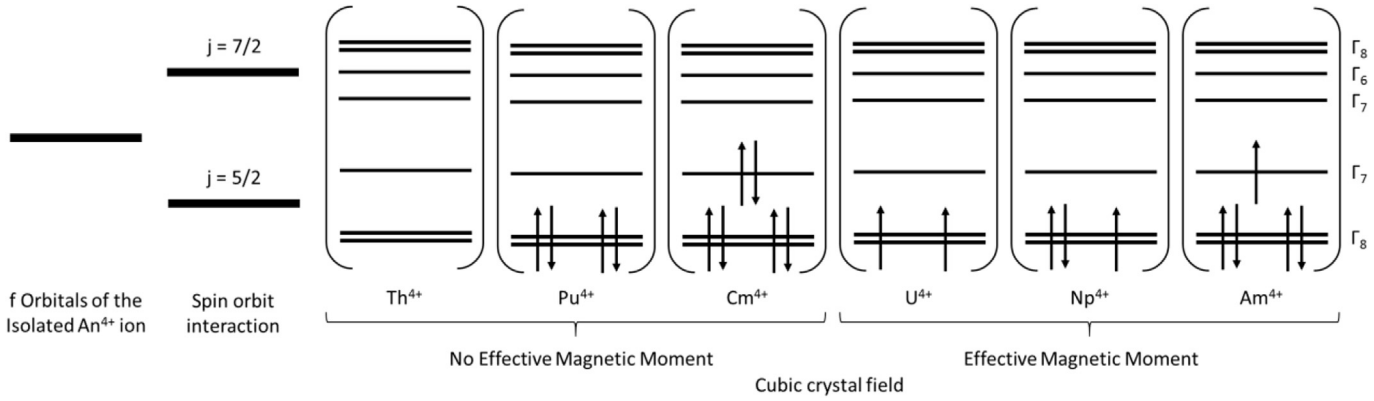

Fig. 2. The one electron splitting of the f orbitals in the cubic crystal field for the AnO_2.

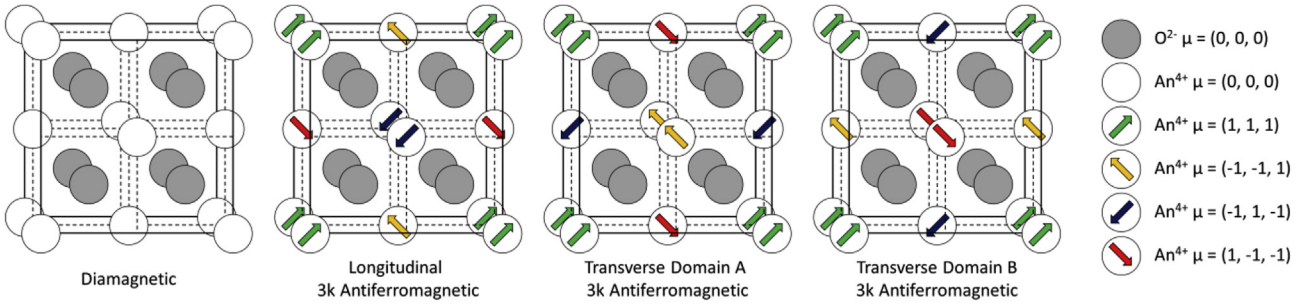

Fig. 3. Illustration of the effective magnetic moments in the AnO_2; diamagnetic, longitudinal 3k antiferromagnetic, transverse domain A 3k antiferromagnetic, and transverse domain B 3k antiferromagnetic.

energetics of the transverse 1-3k AFM states, and has indicated a transverse 3k AFM as the ground state [19], which is the one considered in this study.

In NpO_2 the effective magnetic moment of the ground state remains conspicuously elusive [35,50–52]. Np^{4+} is a Kramers ion [53], an ion with at an odd number of electrons, and therefore should have a magnetic moment. ^{237}Np Mössbauer spectroscopy [50] and muon experiments [35] have thus far established an effective magnetic moment of 0.00–0.15 μ_B/Np^{4+} ion. In the PM phase, $T_N = 60$ K, the effective magnetic moment increases to 2.95 μ_B/Np^{4+} ion [54]. The longitudinal 3k AFM ground state has been inferred from resonant x-ray scattering [36] and ^{17}O NMR [55] studies on NpO_2. Thus, the longitudinal 3k AFM state is employed in these calculations.

Finally, experimental information on the magnetic structure of AmO_2 is extremely limited. Magnetic susceptibility measurements have indicated a AFM ground state (T_N = 8.5 K) although the effective magnetic moment still eludes detection. Conversely, in the PM phase, an effective moment of 1.32 μ_B/Am^{4+} ion at 15–40 K and 1.53 μ_B/Am^{4+} ion at 50–100 K has been measured [56]. Independent Mössbauer and neutron measurements have been unable to provide evidence for a magnetically ordered ground state [57]. In ^{17}O NMR studies on $(Pu_{0.91}Am_{0.09})O_2$ an effective magnetic moment of 1.38 μ_B/Am^{4+} ion is estimated with an internal distortion of the oxygen ions synonymous with transverse 3k AFM order [58]. To our knowledge no study has examined the energetic differences between the longitudinal 3k AFM and transverse 3k AFM phases of AmO_2. Thus, the relative energetics of the longitudinal 3k AFM and the transverse AFM states are compared to establish the magnetic ground state for AmO_2.

2. Computational method

All calculations have been performed using the Vienna Ab-initio Simulation Package (VASP) [19–21], which is based on the density functional theory (DFT) and uses plane wave basis sets. In our convergence tests (Fig. S1) we defined an acceptable kinetic energy cut-off of 500 eV. Our results are derived from the conventional 12 atom unit cell. The description of the reciprocal space was done using the Γ-centred Monkhorst-Pack [59] (5 × 5 x 5) k-point mesh, and the integration over the Brillouin zone was performed using the Blöchl tetrahedron method [60]. In optical absorbance calculations the k-point mesh is (15 × 15 × 15). For the band structure calculations, we define the k-point pathway for the respective $Fm\bar{3}m$ and $Pa\bar{3}$ structures as Γ → L → W → X → Γ and Γ → M → R → X → Γ → R. In this study, we have compared the following exchange-correlation functionals: the local density approximation (LDA) [61,62], and with the general gradient approximation (GGA) of Perdew-Burke-Ernzerhof (PBE) [63], Armiento-Mattsson (AM05) [28,64,65], and PBE revised for solids (PBE-Sol) [66]. We have considered the following explicit electrons for each atomic species: O ($1s^2 2s^2 2p^2$); Th ($5f^1 6s^2 6p^6 6d^1 7s^2$); U ($5f^3 6s^2 6p^6 6d^1 7s^2$); Np ($5f^4 6s^2 6p^6 6d^1 7s^2$); Pu ($5f^5 6s^2 6p^6 6d^1 7s^2$); Am ($5f^6 6s^2 6p^6 6d^1 7s^2$); and Cm ($5f^7 6s^2 6p^6 6d^1 7s^2$). The ion-electron interaction was described using the projector-augmented wave (PAW) approximation [22,23], also considering in our calculations the relativistic spin-orbit interactions (SOI) and magnetic moments as well [67]. All calculations were performed until self-consistency, with electronic and ionic thresholds of $1{\cdot}10^{-7}$ eV and $1{\cdot}10^{-2}$ eV A^{-1} respectively, and with the evaluation of the forces performed by the conjugate gradient algorithm [68]. The correction of the electron self-interaction error implicit in DFT calculations, was assessed by

considering the on-site Coulombic (U) and exchange (J) constant, as described in the rotationally invariant Liechtenstein et al. formulism [69]. These parameters were applied to the *f*-orbitals of the actinide elements. The juxtaposition of energy levels and the presence of meta-stable states makes the determination of the lowest energy configuration for a given magnetic system challenging [70–73]. Here, by analysing trends in the data, and where necessary considering different initial electronic and ionic configurations, we have ensured as far as possible that the lowest energy configurations were obtained.

3. Results & discussion

3.1. Non-ordered magnetic materials

In our discussion, the performance of the functionals is addressed with DFT+U where a range of U = 0.00–7.00 eV is investigated, with J = 0.00 eV. Next, the effect of exchange is investigated further with PBE-Sol for U = 0.00–7.00 eV and J = 0.00–1.00 eV.

The non-ordered AnO_2 materials include ThO_2, PuO_2 and CmO_2. The selection of DFT+U values and the exchange correlation functional focuses first on reproducing the electronic structure as described by the band gap, and second the lattice constant. In general, the functional has little effect on the calculated band gap (Fig. S2), but it, greatly affects the lattice constant (Fig. S3). One further observes the near identical performance of AM05 and PBE-Sol. It is, however, noted that for PuO_2 and CmO_2, the DM state may not be the fundamental magnetic ground state. As already mentioned, this has previously been ascribed to how the exchange-correlation energy is evaluated within the DFT framework [25]. In this paper, our aim is to replicate the properties derived from CF theory in conjunction with experimental analysis.

In ThO_2, the Th^{4+} *f* orbitals to which the U is applied are unoccupied and the DFT+U correction thus has a marginal effect on the electronic structure. Here, the experimental band gap of 5.90 eV [74,75] is systematically underestimated by DFT and DFT+U (Fig. S2a). The AM05/PBE-Sol functionals provided the closest approximation when U = 6.00 eV with a calculated value of 4.70–4.80 eV. This represent an underestimation of 1.10–1.20 eV but it still offers an improvement over previous DFT studies [76,77]. The lattice constant is reproduced by LDA, AM05 and PBE-Sol when U = 3.00–6.00 eV, but remains overestimated by PBE (Fig. S3a).

In PuO_2, the band gap is greatly influenced by the choice of U. In DFT, PuO_2 is calculated in the DM state as a metal; increasing U enables the formation of a band gap. In addition, past DFT studies have additionally reported a FM metallic ground state [78]. Our focus, however, remains on replicating the experimentally derived DM condition. Given the limited experimental information, previous DFT+U studies referenced the band gap from the activation energy for electronic conduction at 1.80 eV [16,70,79,80], but recent measurements of optical absorbance on epitaxial films have reported a band gap of 2.80 eV [81,82]. Assuming the correct band gap is 2.80 eV, this is reproduced by all functionals when U = 6.00–6.50 eV (Fig. S2b). In this range, the lattice constant is best represented by AM05/PBE-Sol (Fig. S3b).

No experimental data has been published on the band gap of CmO_2, although it is believed to be an insulator [12,18,25]. Our calculations also point in that direction. As U is increased CmO_2 transforms from a semi-conductor to an insulator, with a band gap that increases from 0.50 to 2.50 eV for U = 0.00–7.00 eV. Although none of the functionals calculates the experimental lattice constant exactly, an excellent approximation is made by AM05 and PBE-Sol when U = 6.00 eV (Fig. S3c).

In general, the experimental data is best represented by the AM05 and PBE-Sol functionals. Thus, PBE-Sol is used further to investigate the influence of the exchange modifier (J) on the band gap and the lattice constant (Figs. S4–S5). In ThO_2, the introduction of J is negligible with respect to the band gap and only has a minor effect on the lattice constant. In PuO_2, the J value detrimentally affects the band gap, with a reduction of 0.50 eV for every 0.25 eV of J. In fact, the best band-gap fitting is obtained when J = 0.00 eV, with negligible implications to the lattice parameter. Finally, in CmO_2, the J modifier increases the band gap by a maximum of 0.75 eV when J = 0.00–1.00 eV, and again, it has barely any influence on the lattice parameter.

In conclusion, for the non-ordered magnetic AnO_2, we have observed that the PBE-Sol/AM05 functionals, in a combination of high U values with J = 0.00 eV, provide the most accurate reproduction of both band-gaps and lattice constants. Hence, assuming the PBE-Sol functional, we have selected the following U and J parameters for an accurate description of the non-ordered magnetic AnO_2: ThO_2 (U = 6.00 eV, J = 0.00 eV), PuO_2 (U = 6.35 eV, J = 0.00eV) and CmO_2 (U = 6.00 eV, J = 0.00 eV). It is worth noting that the U and J choice for CmO_2 is based upon the better fitting to its lattice parameter, thus predicting a bandgap of 2.50 eV. Using these determined values, we have calculated the following variables: band structure, density of states, optical absorbance spectra, and bulk modulus.

The band structures of ThO_2, PuO_2 and CmO_2 are presented in Fig. 4. In ThO_2, the calculated indirect band gap of 4.63 eV occurs between the respective L and X-Γ points of the valence band maximum (VBM) and conduction band minimum (CBM), compared to the experimental band gap of 5.90 eV [74,75]. In PuO_2, with respect to the band structure, we report a Γ centred direct band gap of 2.81 eV. For CmO_2, an indirect band gap of 2.50 eV is predicted between the respective Γ and L of the VBM and CBM. For ThO_2 and CmO_2, the difference between direct and indirect band gaps is 0.17 eV.

The density of states (DOS) for ThO_2, CmO_2 and PuO_2 are shown in Fig. 5. In each instance the valence band is dominated by the O(p) states with minor contributions from the An(d) and An(f) states. In ThO_2, the conduction band comprises of Th(d), Th(f), and O(p) states, exemplifying the Mott insulator characteristics of ThO_2. In

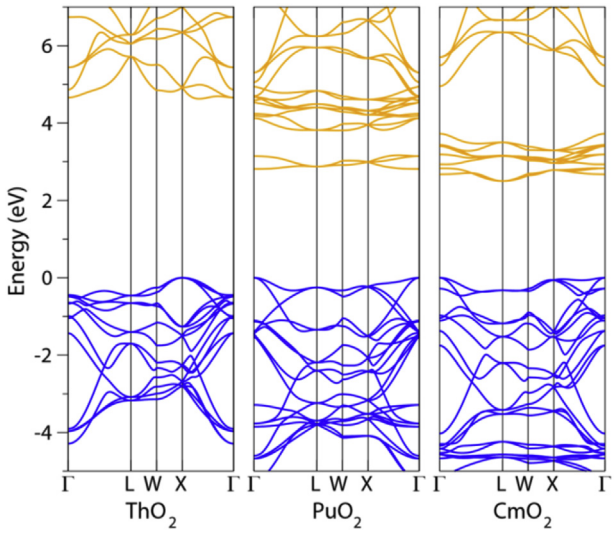

Fig. 4. The calculated effective band structure for ThO_2 ($Fm\bar{3}$ m), PuO_2 ($Fm\bar{3}$ m) and CmO_2 ($Fm\bar{3}$ m). The valence bands are coloured blue whereas the conduction bands are coloured orange. The valence band maximum is set to 0 eV. (For interpretation of the references to colour in this figure legend, the reader is referred to the web version of this article.)

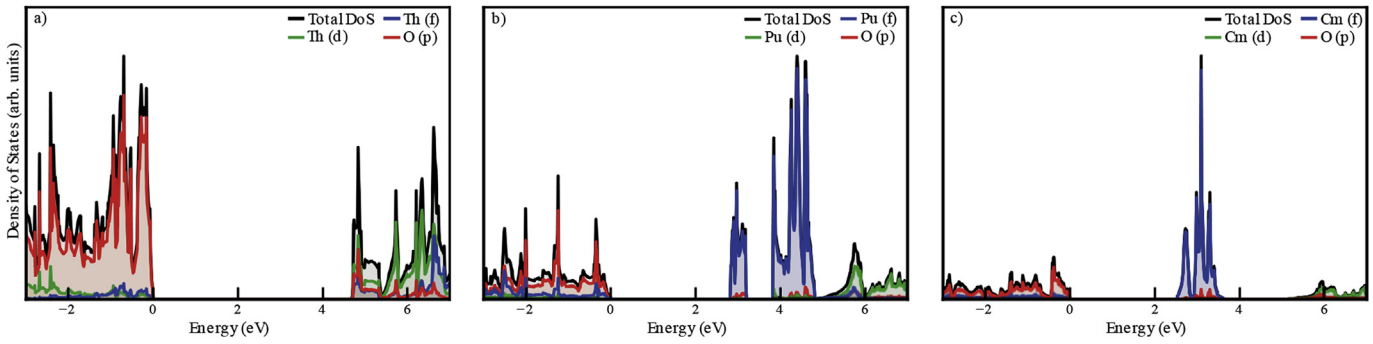

Fig. 5. The calculated density of states for a) ThO_2, b) PuO_2, c) CmO_2. The valence band maximum is set to 0 eV.

PuO_2 and CmO_2, the conduction band is primarily formed from the An(f) states, from which we predict these materials to be charge-transfer insulators where electronic transitions occur across the oxygen and actinide ions.

Whereas the fundamental band gap represents the transition between the VBM and CBM the optical band gap is restricted by orbital symmetry. In recent studies on In_2O_3 [83], AgCuS [84], PbO_2 [85], Tl_2O_3 [86], and $SrCu_2O_2$ [87], it has been shown that the fundamental band gap and optical band gap may differ in value. Our calculated optical absorbance spectra for ThO_2, PuO_2 and CmO_2 are shown in Fig. 6, from which we found that the direct band gap and the optical band gap respectively differ by 0.11 eV, 0.01 eV and 0.19 eV for ThO_2, PuO_2 and CmO_2, as shown in Table 1. Thus, optical absorbance measurements are only representative of the direct band gap in PuO_2.

Finally, the bulk modulus is notoriously difficult to obtain experimentally, which has led to a large range of values in the literature [32,95]. However, our calculated values are in excellent agreement with the experimental data for ThO_2 and CmO_2. For PuO_2, where the reported experimental values for the bulk modulus range from 178 to 379 GPa, our value of 217 GPa provides a useful point of comparison for experimentalists.

3.2. Ordered magnetic materials

Experimental studies of UO_2 and NpO_2 indicate a respective transverse 3k AFM and longitudinal 3k AFM ground state, whereas for AmO_2, to our knowledge, the domain of the 3k AFM ground state is undetermined. Initially, the relative energetics of the transverse 3k AFM and longitudinal 3k AFM states were calculated with PBE-Sol when U = 0.00–7.00 eV and J = 0.00 eV. DFT calculates a longitudinal 3k AFM ground state, but DFT+U (U = 1.00–7.00 eV) calculates a transverse 3k AFM ground state (Table S1). Thus, the transverse 3k AFM ground state is used for further calculations of AmO_2.

As with the non-ordered magnetic AnO_2, the choice of functional has a minor effect on the calculated band gap (Fig. S6) and on the effective An^{4+} magnetic moment (Fig. S7). The sole exception is the band gap of AmO_2; here, when U = 7.00 eV, the LDA functional differs considerably from the GGA functionals. The choice of functional, however, has a pronounced effect on the lattice constants (Fig. S8). The U modifier is the dominating factor for the band gap and the lattice constant, whereas the magnetic moment is only marginally influenced. In order to be consistent with the analysis of the non-ordered magnetic materials, the influence of J was only assessed for the PBE-Sol functional.

In UO_2, the experimental band gap of 2.00–2.50 eV [98–101] is reproduced when U = 3.00–4.00 eV, for all functionals (Fig. S6a). In this range, the experimental lattice constant of 5.470–5.473 Å [32,88,102] is perfectly matched by the AM05/PBE-Sol functionals. The experimental effective magnetic moment of 1.74–1.80 μ_B/U^{4+} ion [48,103] is underestimated by all functionals. In DFT (U = 0 eV) the calculated magnetic moment is found between 0.05 and 1.01 μ_B/U^{4+} ion. In DFT+U, when U = 1.00 eV, it is improved to 1.04–1.41 μ_B/U^{4+} ion. Unfortunately, further increases in U have minimal impact. The introduction of J, only considered for the PBE-Sol, has minimal impact on the band gap (Fig. S9a) and the lattice constant (Fig. S11a). However, J has a detrimental influence on the effective

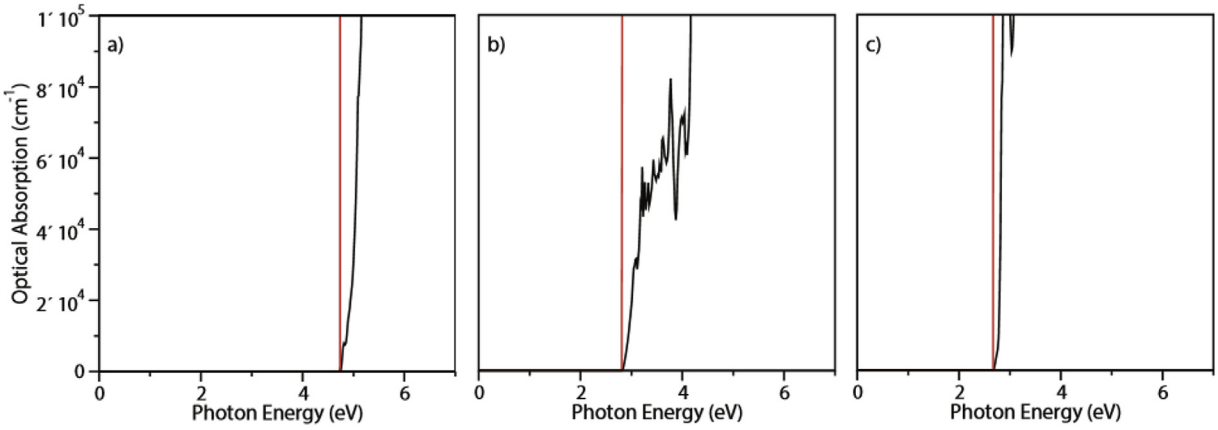

Fig. 6. Calculated optical absorption for a) ThO_2, b) PuO_2, c) CmO_2. The black and red lines respectively represent α (the optical absorption coefficient) and $(\alpha h\nu)^2$ (the optical absorption). (For interpretation of the references to colour in this figure legend, the reader is referred to the web version of this article.)

Table 1
Direct band gap (ΔE_D, eV) and optical band gap (ΔE_O, eV), lattice constant (a_0, in Å) and bulk modulus (B_0, in GPa), for ThO_2, PuO_2, and CmO_2, as calculated in this paper (Calc.) compared to the reported experimental values (Exp.). U and J are expressed in eV and all materials have been calculated as diamagnetic.

AnO_2	DFT+U		ΔE			a_0		B_0	
	U	J	Calc.		Exp.	Calc.	Exp.	Calc.	Exp.
			ΔE_D	ΔE_O					
ThO_2	6.00	0.00	4.63	4.74	5.90 [74,75]	5.637	5.597–5.600 [30,32,88,89]	201	193-198 [32,89,90]
PuO_2	6.00	0.00	2.81	2.82	2.80 [82]	5.411	5.395–5.398 [88,91–94]	217	178 [32] 379 [95]
CmO_2	6.00	0.00	2.50	2.69	–	5.347	5.359–5.372 [93,96]	218	218 [97]

Table 2
Magnetic moment (μ, in μ_B), direct band gap (ΔE_D, eV) and optical band gap (ΔE_O, eV), lattice constant (a_0, in Å), bulk modulus (B_0, in GPa) for UO_2, NpO_2, and AmO_2, as calculated in this paper (Calc.) compared to the reported experimental values (Exp.). U and J are expressed in eV. The transverse 3k AFM state is calculated for UO_2 and AmO_2, whereas, the longitudinal 3k AFM state is calculated for NpO_2.

AnO_2	DFT+U		μ_B		ΔE			a_0		B_0	
	U	J	Calc.	Exp.	Calc.		Exp.	Calc.	Exp.	Calc.	Exp.
					ΔE_D	ΔE_O					
UO_2	3.35	0	1.35	1.74–1.80 [48,103], 3.11 [39]	2.06	2.20	1.30 [115], 2.00–2.50 [98–101]	5.474	5.470–5.473 [32,88,102,116]	210	207 [32]
NpO_2	5.00	0.75	1.87	0.00–0.15 [35,50]	3.08	3.11	2.85–3.10 [82,106]	5.448	5.434 [88,93]	214	200 [32]
AmO_2	7.00	0.50	3.35	1.38 [58]	1.31	1.45	1.30 [106]	5.379	5.372–5.379 [14,30,93,112]	196	205 [32] 280 [97]

U^{4+} magnetic moment (Fig. S10a). Thus, a better correlation between the band gap and the effective U^{4+} magnetic moment is obtained in the absence of J. Hence, for PBE-Sol, U = 3.35 eV and J = 0.00 eV are the appropriate values to describe UO_2, Table 2. Our value of U and J for the transverse 3k AFM ground state is considerably lower the calculated U = 5.7 eV and J = 0.4 eV values obtained explicitly from the constrain random phase approximation (cRPA) method considering collinear 1k AFM order [104]. It is generally accepted that the AnO_2 crystallise in the $Fm\bar{3}$ m motif. However, in UO_2, an internal distortion of the oxygen ions had been reported by a number of studies [37,49,103]. Only recently, rather than oxygen distortion, an alternative $Pa\bar{3}$ symmetry was suggested from neutron diffraction measurements [105]. In our calculations, the transverse 3k AFM ground state is successful in reproducing this subtle $Pa\bar{3}$ symmetry as the lowest-energy structure, in contrast to previous theoretical studies where collinear 1k AFM order was modelled which results in either $Fm\bar{3}$ m symmetry or a distorted $Fm\bar{3}$ m structure. Here, the distortion of 0.016 Å is identical to that derived from neutron diffraction measurements [105].

For NpO_2, the experimental band gap of 2.85–3.10 eV [82,106] is well reproduced by all functionals when U = 5 eV (Fig. S6b), and the experimental lattice constant of 5.434 Å [88,93] is reproduced by PBE (U = 0.00 eV), LDA (U = 3.00–4.00 eV), and AM05/PBE-Sol (U = 6.00–7.00 eV). The effective Np^{4+} magnetic moment, however, remains an enigmatic issue. Our calculated effective Np^{4+} magnetic moment ranges from 2.14 to 2.77μ_B/Np^{4+} ion (Fig. S7b) depending on the functional rather than on the U parameter. However, these values are not compatible with the experimental values since, as indicated by several experimental papers, the magnetic moment is only 0.00–0.15 μ_B/Np^{4+}ion [35,50,51,107–109]. Interestingly, our value does compare with the effective paramagnetic moment of 2.95 μ_B/Np^{4+} ion, determined at 60 K [54]. Focusing now on the PBE-Sol functional, the introduction of J (Figs. S9b–S11b) enables a better correlation between the band gap, effective Np^{4+} magnetic moment and lattice constant when U = 5.00 eV and J = 0.75 eV, as collected in Table 2. Although the calculated effective magnetic moment of 1.87 μ_B/Np^{4+} ion is still overestimated with respect to the longitudinal 3k AFM structure, it offers an improvement over previous investigations [1,7]. Finally, no internal oxygen distortions have been observed in this structure, despite suggestions in some studies [110,111].

In AmO_2, the experimental band gap of 1.30 eV [106] is well reproduced by all the functionals when U = 4.00 eV. Additionally, the band gap is also calculated by the GGA functionals when U = 7.00 eV (Fig. S6c). However, the experimental lattice constant of 5.372–5.379 Å [14,30,93,112] is reproduced only by the AM05/PBE-Sol when U = 4.00–7.00 eV, (Fig. S8c). The experimental effective magnetic moment of 1.38 μ_B/Am^{4+} ion [58] is overestimated by ~3.00 μ_B/Am^{4+} ion regardless of the U value, as depicted in Fig. S7c. The magnetic moment of AmO_2 is small when contrasted against the spin moment. Consequently, we have examined the orbital moments, Table S2. Here, the f orbital is the major contributor to the total magnetic moment of the Am^{4+} ion. It is, however, unclear what causes the reduction in the orbital moment. In the specific case of the PBE-Sol functional, the introduction of J (Figs. S9c–11c) provides a better correlation between the band gap, lattice constant

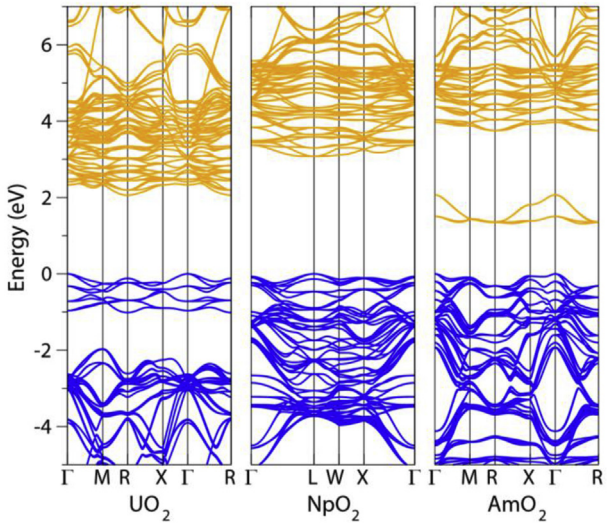

Fig. 7. The calculated effective band structure for UO_2 ($Pa\bar{3}$), NpO_2 ($Fm\bar{3}$ m) and AmO_2 ($Pa\bar{3}$). The valence bands are coloured blue whereas the conduction bands are coloured orange. The valence band maximum is set to 0.00 eV. (For interpretation of the references to colour in this figure legend, the reader is referred to the web version of this article.)

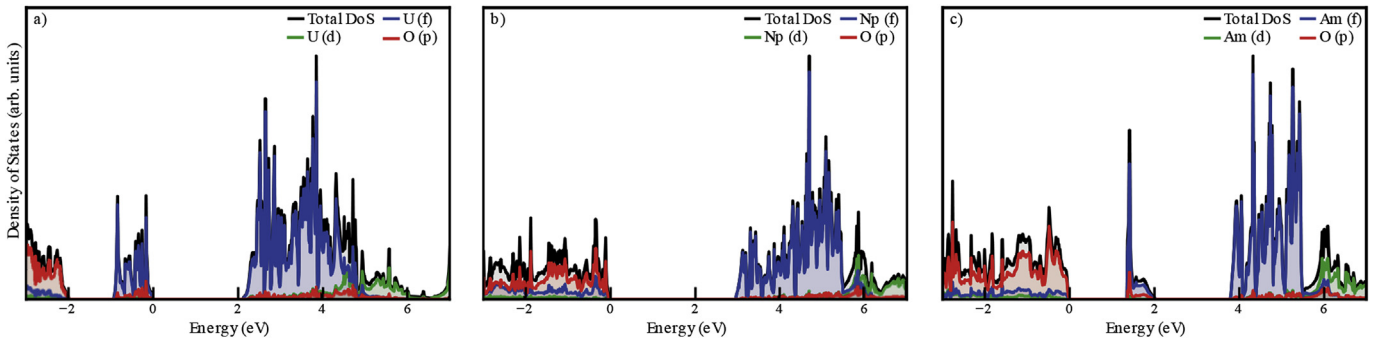

Fig. 8. The calculated density of states for; a) UO_2, b) NpO_2, c) AmO_2. The valence band maximum is set to 0.00 eV.

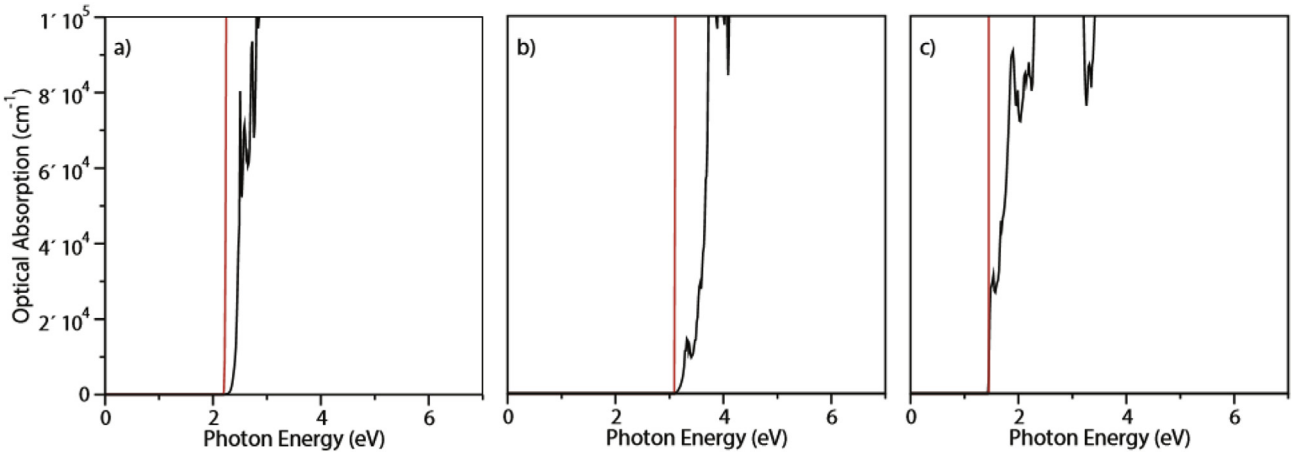

Fig. 9. The calculated optical absorption spectra for; a) UO_2, b) NpO_2, c) AmO_2. The black and red lines respectively represent α (the optical absorption coefficient) and $(\alpha h\nu)^2$ (the optical absorption). (For interpretation of the references to colour in this figure legend, the reader is referred to the web version of this article.)

and the estimated effective Am^{4+} magnetic moment when U = 7.00 eV and J = 0.50 eV. Although the calculated effective Am^{4+} magnetic moment still presents a significant overestimation, it offers an improvement over previous calculations [13,113]. In these DFT+U constraints, the lattice constant is in excellent agreement with the experimental information (see Table 2). Finally, it is noted that the transverse 3k AFM structure produces an internal distortion of the oxygen ions with amplitude 0.082 Å, which is substantially greater that observed in UO_2 (Table 2). The resultant structure therefore possesses $Pa\overline{3}$ symmetry. Unfortunately, the lattice distortion in AmO_2 has not yet been experimentally investigated.

In summary, for the ordered magnetic AnO_2 the AM05/PBE-Sol functionals provide the closest representation of the experimental band gap, effective magnetic moment of the An^{4+} ions and the lattice constant. Thus, from the PBE-Sol functional, the band structure, density of states, optical absorption and bulk modulus are calculated for UO_2 (U = 3.35 eV, J = 0.00 eV), NpO_2 (U = 5.00 eV, J = 0.75 eV) and AmO_2 (U = 7.00 eV, J = 0.50 eV) (Table 2).

The band structures for UO_2, NpO_2 and AmO_2 are shown in Fig. 7. In contrast to their non-ordered magnetic counterparts, the degeneracy of the bands is perturbed for ordered magnetic AnO_2 systems. In UO_2, an indirect band gap of 2.06 eV occurs between Γ and R of the VBM and CBM. For NpO_2, a direct band gap of 3.08 eV occurs at the L point. For AmO_2, an indirect band gap of 1.31 eV occurs between respective Γ and Γ-R of the VBM and CBM respectively.

The DoS for UO_2, NpO_2 and AmO_2 is illustrated in Fig. 8. Unlike NpO_2, AmO_2 and the non-magnetic actinide oxides, in which the valence band is dominated by the O(p) states, UO_2 presents a valence band dominated by U(f) states, clearly indicating that UO_2 is a Mott [100,114] insulator. In each compound the An(f) states contribute heavily to the conduction band. The An(d) states feature more prominently when the energy is greater than 4.00 eV.

The calculated optical absorption spectra for UO_2, NpO_2 and AmO_2 are shown in Fig. 9. The direct band gap and optical band gaps respectively differ by 0.14 eV, 0.03 eV and 0.14 eV for UO_2, NpO_2 and AmO_2, as shown in Table 2. Thus, optical absorbance measurements can only be fully relied upon for the fundamental electronic structure of NpO_2.

Finally, the calculated bulk modulus is in excellent agreement with the experimental data. For AmO_2, the calculated value of 196 GPa offers a point of comparison against the large experimental range of 205–280 GPa.

4. Conclusions

In this paper we have presented a systematic and comprehensive computational study of the actinide oxides: ThO_2, UO_2, NpO_2, PuO_2, AmO_2, and CmO_2. We have compared the performance of the LDA, PBE, AM05 and PBE-Sol functionals in combination with the DFT+U methodology. The choice of functional has little effect on the calculated band gap, but it has a major influence on the lattice constant, bulk modulus and the magnetic moment. In the majority of cases AM05 and PBE-Sol behave in an identical fashion providing the best estimate of the lattice constant. We conclude that either

AM05 or PBE-Sol would provide the best performance in future research of these oxide materials.

The selection of U and J primarily focused on the replication of the magnetic ground state of all oxides to ensure the correct modelling of the magnetic properties as well as the band gap and lattice constants. Where no experimental data was available for AmO_2 we have proposed the longitudinal 3k AFM as the magnetic ground state. For the magnetic ordered oxides, UO_2, NpO_2, AmO_2, U and J were also parametrized to reproduce the effective An^{4+} magnetic moment of the materials. In terms of the lattice, displacement of the oxygen ions results in a Pa-3m structure which is only observed in the transverse 3k AFM structure employed in the calculation of UO_2 and AmO_2 butno such distortion is recorded from the longitudinal 3k AFM for NpO_2.

With the DFT+U parameters determined for each compound, we have also studied other properties like the band-structure, density of states, and the optical band gap. Only for PuO_2 and NpO_2 is excellent agreement found between the fundamental and optical band gap. Furthermore, where it has been generally accepted that the AnO_2 are Mott insulators, only UO_2 displays this characteristic, whereas the remaining AnO_2 are calculated to be charge-transfer insulators. This paper provides the basic tools for future computational study of the actinide dioxides. For instance, surface and doping studies, which are the topic of ongoing research.

Unfortunately, due to experimental limitations, detailed information on elastic constants, cohesive energies and enthalpies of formation are thus far absent from the literature, and our models are therefore strictly justified with respect only to the lattice constants and the electronic properties. As such, this paper offers a guide for theoretical researchers and highlights the need for further experimental information to justify our models. Once new experimental data are reported, these parameters may have to be revised. However, at the moment, this work offers as good a set of parameters to calculate the structures and properties of actinide oxides as can be derived from currently available experimental data.

Acknowledgements

This research was supported by the UK Engineering & Physical Science Research Council (Grant nos. EP/G036675 and EP/K016288) and the Atomic Weapons Establishment. The authors thank Alex Ganose and David Scanlon for valuable discussions. N.H.dL. would like to thank the Royal Society for an Industry Fellowship and AWE for a William Penney Fellowship. Finally, J.T.P. thanks Jacqueline Dwomoh Nana Manu for her kindness, support and insight.

Appendix A. Supplementary data

Supplementary data related to this article can be found at http://dx.doi.org/10.1016/j.jnucmat.2017.05.025.

References

[1] X.-D. Wen, R.L. Martin, T.M. Henderson, G.E. Scuseria, Density functional theory studies of the electronic structure of solid state actinide oxides, Chem. Rev. 113 (2) (2012) 1063–1096.
[2] G.R. Choppin, J.-O. Liljenzin, J.A.N. Rydberg, CHAPTER 1-Origin of Nuclear Science, Radiochemistry and Nuclear Chemistry, third ed., Butterworth-Heinemann, Woburn, 2002, pp. 1–10.
[3] D. Olander, Nuclear fuels – present and future, J. Nucl. Mater. 389 (1) (2009) 1–22.
[4] J.M. Haschke, T.H. Allen, J.C. Martz, Oxidation kinetics of plutonium in air: consequences for environmental dispersal, J. Alloys Compd. 271–273 (1998) 211–215.
[5] D.A. Andersson, J. Lezama, B.P. Uberuaga, C. Deo, S.D. Conradson, Cooperativity among defect sites in AO_{2+x} and A_4O_9 (A=U,Np,Pu): density functional calculations, Phys. Rev. B 79 (2) (2009) 024110.
[6] Y. Yang, B. Wang, P. Zhang, Electronic and mechanical properties of ordered $(Pu,U)O_2$ compounds: a density functional theory +U study, J. Nucl. Mater. 433 (1–3) (2013) 345–350.
[7] B.-T. Wang, H. Shi, W. Li, P. Zhang, First-principles LDA+U and GGA+U study of neptunium dioxide, Phys. Rev. B 81 (4) (2010) 045119.
[8] S.A. Moten, R. Atta-Fynn, A.K. Ray, M.N. Huda, Size effects on the electronic and magnetic properties of PuO2(111) surface, J. Nucl. Mater. 468 (2016) 37–45.
[9] C. Guéneau, N. Dupin, B. Sundman, C. Martial, J.-C. Dumas, S. Gossé, S. Chatain, F.D. Bruycker, D. Manara, R.J.M. Konings, Thermodynamic modelling of advanced oxide and carbide nuclear fuels: description of the U–Pu–O–C systems, J. Nucl. Mater. 419 (1–3) (2011) 145–167.
[10] L.R. Morss, N. Edelstein, J. Fuger, J.J. Katz, The Chemistry of the Actinide and Transactinide Elements, fourth ed., Springer, 2011.
[11] E. Kotomin, Y.A. Mastrikov, Y.F. Zhukovskii, P. Van Uffelen, V. Rondinella, First-principles modelling of defects in advanced nuclear fuels, Phys. status solidi C. 4 (3) (2007) 1193–1196.
[12] L. Petit, A. Svane, Z. Szotek, W.M. Temmerman, G.M. Stocks, Electronic structure and ionicity of actinide oxides from first principles, Phys. Rev. B 81 (4) (2010) 045108.
[13] Y. Lu, Y. Yang, F. Zheng, B.-T. Wang, P. Zhang, Electronic, mechanical, and thermodynamic properties of americium dioxide, J. Nucl. Mater. 441 (1–3) (2013) 411–420.
[14] T. Nishi, M. Nakada, A. Itoh, C. Suzuki, M. Hirata, M. Akabori, EXAFS and XANES studies of americium dioxide with fluorite structure, J. Nucl. Mater. 374 (3) (2008) 339–343.
[15] C. Suzuki, T. Nishi, M. Nakada, T. Tsuru, M. Akabori, M. Hirata, Y. Kaji, DFT study on the electronic structure and chemical state of Americium in an (Am,U) mixed oxide, J. Phys. Chem. Solids 74 (12) (2013) 1769–1774.
[16] I.D. Prodan, G.E. Scuseria, J.A. Sordo, K.N. Kudin, R.L. Martin, Lattice defects and magnetic ordering in plutonium oxides: a hybrid density-functional-theory study of strongly correlated materials, J. Chem. Phys. 123 (1) (2005) 014703.
[17] L. Jin, P. Li, X. Lei, H. Zhou, C. Wang, Mechanical and thermal properties of NpO2 using LSDA+U approach, Prog. Nat. Sci. Mater. Int. 24 (4) (2014) 373–377.
[18] I.D. Prodan, G.E. Scuseria, R.L. Martin, Covalency in the actinide dioxides: systematic study of the electronic properties using screened hybrid density functional theory, Phys. Rev. B 76 (3) (2007) 033101.
[19] D. Gryaznov, E. Heifets, D. Sedmidubsky, Density functional theory calculations on magnetic properties of actinide compounds, Phys. Chem. Chem. Phys. 12 (38) (2010) 12273–12278.
[20] J.P. Perdew, A. Zunger, Self-interaction correction to density-functional approximations for many-electron systems, Phys. Rev. B 23 (10) (1981) 5048–5079.
[21] V.I. Anisimov, A.I. Lichtenstein, V.I. Anisimov, Strong Coulomb Correlations in Electronic Structure Calculations: beyond the Local Density Approximation, 2000.
[22] A. Georges, G. Kotliar, W. Krauth, M.J. Rozenberg, Dynamical mean-field theory of strongly correlated fermion systems and the limit of infinite dimensions, Rev. Mod. Phys. 68 (1) (1996) 13–125.
[23] J. Heyd, G.E. Scuseria, M. Ernzerhof, Hybrid functionals based on a screened Coulomb potential, J. Chem. Phys. 118 (18) (2003) 8207–8215.
[24] J. Heyd, G.E. Scuseria, M. Ernzerhof, Erratum: "Hybrid functionals based on a screened Coulomb potential" [J. Chem. Phys.118, 8207 (2003)], J. Chem. Phys. 124 (21) (2006) 219906.
[25] M.T. Suzuki, N. Magnani, P.M. Oppeneer, Microscopic theory of the insulating electronic ground states of the actinide dioxides AnO_2 (An = U, Np, Pu, Am, and Cm), Phys. Rev. B 88 (19) (2013) 195146.
[26] P. Giannozzi, P. Erdös, Theoretical analysis of the 3-k magnetic structure and distortion of uranium dioxide, J. Magnetism Magnetic Mater. 67 (1) (1987) 75–87.
[27] R. Laskowski, G.K.H. Madsen, P. Blaha, K. Schwarz, Magnetic structure and electric-field gradients of uranium dioxide: an *ab initio* study, Phys. Rev. B 69 (14) (2004) 140408.
[28] A.E. Mattsson, R. Armiento, J. Paier, G. Kresse, J.M. Wills, T.R. Mattsson, The AM05 density functional applied to solids, J. Chem. Phys. 128 (8) (2008) 084714.
[29] M. Ropo, K. Kokko, L. Vitos, Assessing the Perdew-Burke-Ernzerhof exchange-correlation density functional revised for metallic bulk and surface systems, Phys. Rev. B 77 (19) (2008) 195445.
[30] T.D. Chikalla, L. Eyring, Phase relationships in the americium-oxygen system, J. Inorg. Nucl. Chem. 30 (1) (1968) 133–145.
[31] J.A. Fahey, R.P. Turcotte, T.D. Chikalla, Thermal expansion of the actinide dioxides, Inorg. Nucl. Chem. Lett. 10 (6) (1974) 459–465.
[32] M. Idiri, T. Le Bihan, S. Heathman, J. Rebizant, Behavior of actinide dioxides under pressure: UO2 and ThO_2, Phys. Rev. B 70 (1) (2004) 014113.
[33] J.M. Fournier, A. Blaise, G. Amoretti, R. Caciuffo, J. Larroque, M.T. Hutchings, R. Osborn, A.D. Taylor, High-energy-neutron spectroscopy of crystal-field excitations in NpO_2, Phys. Rev. B 43 (1) (1991) 1142–1145.
[34] R. Caciuffo, N. Magnani, P. Santini, S. Carretta, G. Amoretti, E. Blackburn, M. Enderle, P.J. Brown, G.H. Lander, Anisotropic magnetic fluctuations in 3-k antiferromagnets, Part 2, J. Magnetism Magnetic Mater. 310 (2) (2007) 1698–1702.
[35] W. Kopmann, F.J. Litterst, H.H. Klauß, M. Hillberg, W. Wagener, G.M. Kalvius, E. Schreier, F.J. Burghart, J. Rebizant, G.H. Lander, Magnetic order in NpO_2 and

UO_2 studied by muon spin rotation, J. Alloys Compd. 271–273 (1998) 463–466.
[36] S.B. Wilkins, J.A. Paixão, R. Caciuffo, P. Javorsky, F. Wastin, J. Rebizant, C. Detlefs, N. Bernhoeft, P. Santini, G.H. Lander, Resonant x-ray scattering study of magnetic-dipole and electric-quadrupole order in $U_{0.75}Np_{0.25}O_2$, Phys. Rev. B 70 (21) (2004) 214402.
[37] P. Santini, R. Lémanski, P. Erdős, Magnetism of actinide compounds, Adv. Phys. 48 (5) (1999) 537–653.
[38] K. Ikushima, S. Tsutsui, Y. Haga, H. Yasuoka, R.E. Walstedt, N.M. Masaki, A. Nakamura, S. Nasu, Y. Ōnuki, First-order phase transition in UO_2: ^{235}U and ^{17}O NMR study, Phys. Rev. B 63 (10) (2001) 104404.
[39] D. Hudry, J.-C. Griveau, C. Apostolidis, O. Walter, E. Colineau, G. Rasmussen, D. Wang, V. Chakravadhaluna, E. Courtois, C. Kübel, D. Meyer, Thorium/uranium mixed oxide nanocrystals: synthesis, structural characterization and magnetic properties, Nano Res. 7 (1) (2014) 119–131.
[40] G. Raphael, R. Lallement, Susceptibilite magnetique de PuO_2, Solid State Commun. 6 (6) (1968) 383–385.
[41] Y. Tokunaga, H. Sakai, T. Fujimoto, S. Kambe, R.E. Walstedt, K. Ikushima, H. Yasuoka, D. Aoki, Y. Homma, Y. Haga, T.D. Matsuda, S. Ikeda, E. Yamamoto, A. Nakamura, Y. Shiokawa, K. Nakajima, Y. Arai, Y. Ōnuki, NMR studies of actinide dioxides, J. Alloys Compd. 444–445 (2007) 241–245.
[42] S. Kern, C.K. Loong, G.L. Goodman, B. Cort, G.H. Lander, Crystal-field spectroscopy of PuO_2 : further complications in actinide dioxides, J. Phys. Condens. Matter 2 (7) (1990) 1933.
[43] S. Kern, R. Robinson, H. Nakotte, G. Lander, B. Cort, P. Watson, F. Vigil, Crystal-field transition in PuO_2, Phys. Rev. B 59 (1) (1999) 104.
[44] H. Yasuoka, G. Koutroulakis, H. Chudo, S. Richmond, D.K. Veirs, A.I. Smith, E.D. Bauer, J.D. Thompson, G.D. Jarvinen, D.L. Clark, Observation of ^{239}Pu nuclear magnetic resonance, Science 336 (6083) (2012) 901–904.
[45] F. Gendron, J. Autschbach, Puzzling lack of temperature dependence of the PuO_2 magnetic susceptibility explained according to ab intio wave function calculations, J. Phys. Chem. Lett. (2017) 673–678.
[46] F. Niikura, T. Hotta, Magnetic behavior of curium dioxide with a nonmagnetic ground state, Phys. Rev. B 83 (17) (2011) 172402.
[47] S.B. Wilkins, R. Caciuffo, C. Detlefs, J. Rebizant, E. Colineau, F. Wastin, G.H. Lander, Direct observation of electric-quadrupolar order in UO_2, Phys. Rev. B 73 (6) (2006) 060406.
[48] B. Frazer, G. Shirane, D. Cox, C. Olsen, Neutron-diffraction study of antiferromagnetism in UO_2, Phys. Rev. 140 (4A) (1965) A1448.
[49] J. Faber, G.H. Lander, B.R. Cooper, Neutron-diffraction study of UO_2: observation of an internal distortion, Phys. Rev. Lett. 35 (26) (1975) 1770–1773.
[50] B.D. Dunlap, G.M. Kalvius, D.J. Lam, M.B. Brodsky, Hyperfine field of ^{237}Np in NpO_2, J. Phys. Chem. Solids 29 (8) (1968) 1365–1367.
[51] D.E. Cox, B.C. Frazer, A neutron diffraction study of NpO_2, J. Phys. Chem. Solids 28 (9) (1967) 1649–1650.
[52] L. Heaton, M.H. Mueller, J.M. Williams, A neutron diffraction determination of the coherent scattering amplitude of NP and the possible antiferromagnetism of neptunium dioxide, J. Phys. Chem. Solids 28 (9) (1967) 1651–1654.
[53] A. Nikolaev, K. Michel, The Structural Phase Transition and Loss of Magnetic Moments in NpO_2: Ab Initio Approach to the Crystal and Mean Field, ArXiv Preprint Cond-mat/0212521, 2002.
[54] J.W. Ross, D.J. Lam, The magnetic susceptibility of neptunium oxide and carbide between 4.2° and 350°K, J. Appl. Phys. 38 (3) (1967) 1451–1453.
[55] Y. Tokunaga, Y. Homma, S. Kambe, D. Aoki, H. Sakai, E. Yamamoto, A. Nakamura, Y. Shiokawa, R.E. Walstedt, H. Yasuoka, NMR evidence for triple-q multipole structure in NpO_2, Phys. Rev. Lett. 94 (13) (2005) 137209.
[56] D.G. Karraker, Magnetic susceptibility of $^{243}AmO_2$, J. Chem. Phys. 63 (7) (1975) 3174–3175.
[57] A. Bœuf, J.M. Fournier, J.F. Gueugnon, L. Manes, J. Rebizant, F. Rustichelli, Neutron diffraction study of $^{243}AmO_2$, J. Phys. Lett. 40 (14) (1979) 335–338.
[58] Y. Tokunaga, M. Osaka, S. Kambe, S. Miwa, H. Sakai, H. Chudo, Y. Homma, Y. Shiokawa, ^{17}O NMR study in $(Pu_{0.91}Am_{0.09})O_2$, J. Nucl. Mater. 396 (1) (2010) 107–111.
[59] H.J. Monkhorst, J.D. Pack, Special points for Brillouin-zone integrations, Phys. Rev. B 13 (12) (1976) 5188–5192.
[60] P.E. Blöchl, O. Jepsen, O.K. Andersen, Improved tetrahedron method for Brillouin-zone integrations, Phys. Rev. B 49 (23) (1994) 16223–16233.
[61] W. Kohn, L.J. Sham, Self-consistent equations including exchange and correlation effects, Phys. Rev. 140 (4A) (1965) A1133–A1138.
[62] J.P. Perdew, Y. Wang, Accurate and simple analytic representation of the electron-gas correlation energy, Phys. Rev. B 45 (23) (1992) 13244–13249.
[63] J.P. Perdew, K. Burke, M. Ernzerhof, Generalized gradient approximation made simple, Phys. Rev. Lett. 77 (18) (1996) 3865–3868.
[64] R. Armiento, A.E. Mattsson, Functional designed to include surface effects in self-consistent density functional theory, Phys. Rev. B 72 (8) (2005) 085108.
[65] A.E. Mattsson, R. Armiento, Implementing and testing the AM05 spin density functional, Phys. Rev. B 79 (15) (2009) 155101.
[66] G.I. Csonka, J.P. Perdew, A. Ruzsinszky, P.H.T. Philipsen, S. Lebègue, J. Paier, O.A. Vydrov, J.G. Ángyán, Assessing the performance of recent density functionals for bulk solids, Phys. Rev. B 79 (15) (2009) 155107.
[67] S. Steiner, S. Khmelevskyi, M. Marsmann, G. Kresse, Calculation of the magnetic anisotropy with projected-augmented-wave methodology and the case study of disordered $Fe_{1-x}Co_x$ alloys, Phys. Rev. B 93 (22) (2016) 224425.
[68] W.H. Press, S.A. Teukolsky, W.T. Vetterling, B.P. Flannery, Numerical Recipes 3rd Edition: the Art of Scientific Computing, Cambridge University Press, 2007.
[69] A.I. Liechtenstein, V.I. Anisimov, J. Zaanen, Density-functional theory and strong interactions: orbital ordering in Mott-Hubbard insulators, Phys. Rev. B 52 (8) (1995) R5467–R5470.
[70] G. Jomard, B. Amadon, F. Bottin, M. Torrent, Structural, thermodynamic, and electronic properties of plutonium oxides from first principles, Phys. Rev. B 78 (7) (2008) 075125.
[71] B. Dorado, M. Freyss, B. Amadon, M. Bertolus, G. Jomard, P. Garcia, Advances in first-principles modelling of point defects in UO_2: f electron correlations and the issue of local energy minima, J. Phys. Condens. Matter 25 (33) (2013) 333201.
[72] B. Meredig, A. Thompson, H.A. Hansen, C. Wolverton, A. van de Walle, Method for locating low-energy solutions within DFT+U, Phys. Rev. B 82 (19) (2010) 195128.
[73] H.Y. Geng, Y. Chen, Y. Kaneta, M. Kinoshita, Q. Wu, Interplay of defect cluster and the stability of xenon in uranium dioxide from density functional calculations, Phys. Rev. B 82 (9) (2010) 094106.
[74] T.R. Griffiths, J. Dixon, Electron irradiation of single crystal thorium dioxide and electron transfer reactions, Inorganica Chim. Acta 300–302 (0) (2000) 305–313.
[75] R.W. Evans, C.S. Barton, M. Clemens, D.D. Allred, Understanding DC-Bias Sputtered Thorium Oxide Thin Films Useful in EUV Optics, SPIE - The International Society of Optical Engineering, 2006.
[76] C. Sevik, T. Çağın, Mechanical and electronic properties of CeO_2, ThO_2, and $(Ce, Th)O_2$ alloys, Phys. Rev. B 80 (1) (2009) 014108.
[77] B.-T. Wang, H. Shi, W.-D. Li, P. Zhang, First-principles study of ground-state properties and high pressure behavior of ThO_2, J. Nucl. Mater. 399 (2) (2010) 181–188.
[78] I.D. Prodan, G.E. Scuseria, R.L. Martin, Assessment of metageneralized gradient approximation and screened Coulomb hybrid density functionals on bulk actinide oxides, Phys. Rev. B 73 (4) (2006) 045104.
[79] P. Zhang, B.-T. Wang, X.-G. Zhao, Ground-state properties and high-pressure behavior of plutonium dioxide: density functional theory calculations, Phys. Rev. B 82 (14) (2010) 144110.
[80] A. Shick, J. Kolorenč, L. Havela, T. Gouder, R. Caciuffo, Nonmagnetic ground state of PuO_2, Phys. Rev. B 89 (4) (2014) 041109.
[81] B.L. Scott, J.J. Joyce, T.D. Durakiewicz, R.L. Martin, T.M. McCleskey, E. Bauer, H. Luo, Q. Jia, High quality epitaxial thin films of actinide oxides, carbides, and nitrides: advancing understanding of electronic structure of f-element materials, Coord. Chem. Rev. 266–267 (0) (2014) 137–154.
[82] T.M. McCleskey, E. Bauer, Q. Jia, A.K. Burrell, B.L. Scott, S.D. Conradson, A. Mueller, L. Roy, X. Wen, G.E. Scuseria, Optical band gap of NpO_2 and PuO_2 from optical absorbance of epitaxial films, J. Appl. Phys. 113 (1) (2013) 013515.
[83] D.O. Scanlon, A. Regoutz, R.G. Egdell, D.J. Morgan, G.W. Watson, Band gap engineering of In_2O_3 by alloying with Tl_2O_3, Appl. Phys. Lett. 103 (26) (2013) 262108.
[84] C.N. Savory, A.M. Ganose, W. Travis, R.S. Atri, R.G. Palgrave, D.O. Scanlon, An assessment of silver copper sulfides for photovoltaic applications: theoretical and experimental insights, J. Mater. Chem. A 4 (32) (2016) 12648–12657.
[85] D.O. Scanlon, A.B. Kehoe, G.W. Watson, M.O. Jones, W.I.F. David, D.J. Payne, R.G. Egdell, P.P. Edwards, A. Walsh, Nature of the band gap and origin of the conductivity of PbO_2 revealed by theory and experiment, Phys. Rev. Lett. 107 (24) (2011) 246402.
[86] A.B. Kehoe, D.O. Scanlon, G.W. Watson, Nature of the band gap of Tl_2O_3, Phys. Rev. B 83 (23) (2011) 233202.
[87] K.G. Godinho, J.J. Carey, B.J. Morgan, D.O. Scanlon, G.W. Watson, Understanding conductivity in $SrCu_2O_2$: stability, geometry and electronic structure of intrinsic defects from first principles, J. Mater. Chem. 20 (6) (2010) 1086–1096.
[88] T. Yamashita, N. Nitani, T. Tsuji, H. Inagaki, Thermal expansions of NpO_2 and some other actinide dioxides, J. Nucl. Mater. 245 (1) (1997) 72–78.
[89] J.S. Olsen, L. Gerward, V. Kanchana, G. Vaitheeswaran, The bulk modulus of ThO_2 - an experimental and theoretical study, J. alloys Compd. 381 (1) (2004) 37–40.
[90] P. Macedo, W. Capps, J. WACHTMAN, Elastic constants of single crystal ThO_2 at 25°C, J. Am. Ceram. Soc. 47 (12) (1964) 651, 651.
[91] T. Yamashita, H. Muto, T. Tsuji, Y. Nakamura, Thermal expansion of neptunium–plutonium mixed oxides, J. Alloys Compd. 271–273 (1998) 404–407.
[92] M. Noe, J. Fuger, Self-radiation effects on the lattice parameter of $^{238}PuO_2$, Inorg. Nucl. Chem. Lett. 10 (1) (1974) 7–19.
[93] L. Asprey, F. Ellinger, S. Fried, W. Zachariasen, Evidence for quadrivalent curium: X-Ray data on curium oxides, J. Am. Chem. Soc. 77 (6) (1955) 1707–1708.
[94] J.M. Haschke, T.H. Allen, L.A. Morales, Reaction of plutonium dioxide with water: formation and properties of PuO_{2+x}, Science 287 (5451) (2000) 285–287.
[95] J.P. Dancausse, E. Gering, S. Heathman, U. Benedict, Pressure-induced phase transition in ThO_2 and PuO_2, High Press. Res. 2 (5–6) (1990) 381–389.
[96] M. Noe, J. Fuger, Self-radiation effects on the lattice parameter of $^{244}CmO_2$, Inorg. Nucl. Chem. Lett. 7 (5) (1971) 421–430.
[97] J. Dancausse, R. Haire, S. Heathman, U. Benedict, High-Pressure x-ray diffraction studies of americium and curium dioxides, J. Nucl. Sci. Technol. 39 (sup3) (2002) 136–139.
[98] T.T. Meek, B. von Roedern, P.G. Clem, R.J. Hanrahan Jr., Some optical

properties of intrinsic and doped UO_2 thin films, Mater. Lett. 59 (8–9) (2005) 1085–1088.
[99] J. Schoenes, Electronic transitions, crystal field effects and phonons in UO_2, Phys. Rep. 63 (6) (1980) 301–336.
[100] S.W. Yu, J.G. Tobin, J.C. Crowhurst, S. Sharma, J.K. Dewhurst, P. Olalde-Velasco, W.L. Yang, W.J. Siekhaus, f-f origin of the insulating state in uranium dioxide: X-ray absorption experiments and first-principles calculations, Phys. Rev. B 83 (16) (2011) 165102.
[101] J. Schoenes, Optical properties and electronic structure of UO_2, J. Appl. Phys. 49 (3) (1978) 1463–1465.
[102] T. Yamashita, N. Nitani, T. Tsuji, T. Kato, Thermodynamics of Nuclear MaterialsThermal expansion of neptunium-uranium mixed oxides, J. Nucl. Mater. 247 (1997) 90–93.
[103] J. Faber, G.H. Lander, Neutron diffraction study of UO2: antiferromagnetic state, Phys. Rev. B 14 (3) (1976) 1151–1164.
[104] B. Amadon, T. Applencourt, F. Bruneval, Screened Coulomb interaction calculations: cRPA implementation and applications to dynamical screening and self-consistency in uranium dioxide and cerium, Phys. Rev. B 89 (12) (2014) 125110.
[105] L. Desgranges, Y. Ma, P. Garcia, G. Baldinozzi, D. Siméone, H.E. Fischer, What is the actual local crystalline structure of uranium dioxide, UO2? A new perspective for the most used nuclear fuel, Inorg. Chem. 56 (1) (2016) 321–326.
[106] C. Suzuki, T. Nishi, M. Nakada, M. Akabori, M. Hirata, Y. Kaji, Core-hole effect on XANES and electronic structure of minor actinide dioxides with fluorite structure, J. Phys. Chem. Solids 73 (2) (2012) 209–216.
[107] J.M. Friedt, F.J. Litterst, J. Rebizant, 25-K phase transition in NpO_2 from ^{237}Np Mössbauer spectroscopy, Phys. Rev. B 32 (1) (1985) 257–263.
[108] A. Delapalme, M. Forte, J.M. Fournier, J. Rebizant, J.C. Spirlet, Induced magnetic form factor of NpO_2, Phys. B+C 102 (1) (1980) 171–173.
[109] P. Erdös, G. Solt, Z. ⊙ołnierek, A. Blaise, J.M. Fournier, Magnetic susceptibility and the phase transition of NpO_2, Phys. B+C 102 (1) (1980) 164–170.
[110] R. Caciuffo, G. Amoretti, J.M. Fournier, A. Blaise, R. Osborn, A.D. Taylor, J. Larroque, M.T. Hutchings, Evidence of a lattice distortion in NpO_2 below 25 K from neutron magnetic inelastic scattering, Solid State Commun. 79 (2) (1991) 197–200.
[111] D. Mannix, G.H. Lander, J. Rebizant, R. Caciuffo, N. Bernhoeft, E. Lidström, C. Vettier, Unusual magnetism of NpO_2: a study with resonant x-ray scattering, Phys. Rev. B 60 (22) (1999) 15187–15193.
[112] C. Hurtgen, J. Fuger, Self-irradiation effects in americium oxides, Inorg. Nucl. Chem. Lett. 13 (3) (1977) 179–188.
[113] X.-D. Wen, R.L. Martin, L.E. Roy, G.E. Scuseria, S.P. Rudin, E.R. Batista, T.M. McCleskey, B.L. Scott, E. Bauer, J.J. Joyce, Effect of spin-orbit coupling on the actinide dioxides AnO_2 (An= Th, Pa, U, Np, Pu, and Am): A screened hybrid density functional study, J. Chem. Phys. 137 (15) (2012) 154707.
[114] N.F. Mott, The basis of the electron theory of metals, with special reference to the transition metals, Proc. Phys. Soc. Sect. A 62 (7) (1949) 416.
[115] T. Meek, M. Hu, M.J. Haire, Semiconductive properties of uranium oxides, ORNL 10 (6) (2001) 10–18.
[116] J. Crowhurst, J. Jeffries, D. Åberg, J. Zaug, Z. Dai, W. Siekhaus, N. Teslich, K. Holliday, K. Knight, A. Nelson, A combined theoretical and experimental investigation of uranium dioxide under high static pressure, J. Phys. Condens. Matter 27 (26) (2015) 265401.